Stereo Reconstruction of the Epicardium for Optical Fluorescence Imaging

Desmond Chung[1], Mihaela Pop[1], Maxime Sermesant[2], Graham A. Wright[1]

[1] Department of Medical Biophysics, University of Toronto,
Sunnybrook Health Sciences Centre, Toronto, Canada
[2] INRIA Sophia Antipolis, France and King's College, London, UK

Email: dchung@swri.ca

Abstract Optical imaging using voltage-sensitive fluorescence dye can record cardiac electrical activity with sub-millimeter resolution that is unattainable with conventional electrode systems. The interpretations of activation recordings are often limited by the two-dimensionality of the maps obtained from the 2D optical images, and little has been done to overcome this limitation. We present a novel method to simultaneously estimate the activation patterns derived from fluorescence images and the 3D geometry of the heart by using a stereo camera configuration. Our results suggest that the stereo reconstruction is feasible in large hearts and may enable a more realistic visualization of propagation of cardiac electrical waves.

1 Introduction

Optical imaging using voltage-sensitive fluorescence dye has become a powerful research tool in studying cardiac arrhythmias [1]; however, the reconstructed maps of the action potential (AP) propagation on the epicardium are often limited to 2D projections. Moreover, the speed of propagation depends on the curvature polarization front, which cannot be correctly estimated from a 2D projection. Recently, this limitation was overcome by using 2 CCD cameras: one mapping the changes in AP and the other capturing the 3D geometry of the heart [2,3]. Simultaneously recovering the 3D epicardial geometry with the AP propagation patterns allows this information to be mapped onto theoretical 3D models of cardiac electrical activity. We present a novel method to simultaneously estimate the activation patterns derived from fluorescence images and 3D geometry of the heart by using a stereo camera configuration. The realistic 3D reconstruction could potentially allow for the validation of 3D theoretical predictions of AP propagation in a point-by-point comparison of simulation results against experimental measurements.

2 Method

We begin by describing the methodology used to record the optical fluorescence images, and then detail the steps used to reconstruct the epicardium in 3D from the stereo optical image pairs.

2.1 Optical Imaging

Optical fluorescence images of the AP propagation were obtained in swine hearts (approximately 8cm long), using a Langendorff ex-vivo perfusion preparation at 37ºC. A schematic of the experimental set-up is shown in Figure 1. The hearts were paced at 60 beats per minute via a bipolar electrode placed inside the ventricle, at the apex. The fluorescence dye (0.2ml sol. di-4-ANEPPS, Biotium Inc.) was dissolved in 20ml of perfusate, and injected continuously over 10 minutes into the coronary system. The dye was excited at 531nm ±20nm through a green filter (FF01-531/40-25, Semrock Inc., Rochester, NY, USA) with two 150W halogen lamps (MHF G150LR, Moritek Corp., Japan). The lamps were controlled by shutters (labeled 'S' in the schematic below) to avoid dye photo-bleaching. The emitted signal was passed through a >610nm high-pass filter and recorded with 2 high-speed CCDs (MiCAM02, BrainVison Inc., Japan).

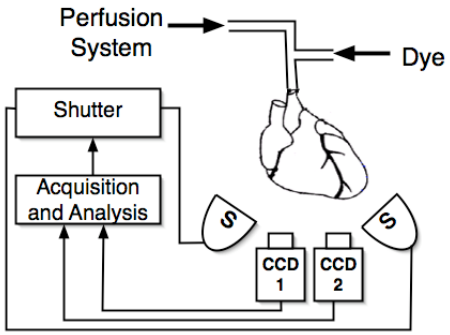

Figure 1. The experimental set-up used for stereo optical fluorescence imaging, with the halogen light sources labeled 'S'.

Fluorescence images of the epicardial surface were captured at 270 frames per second over 192x128 pixels, yielding a spatial resolution of less than 0.7mm, and a temporal resolution of 3.7ms. The action potential is given by the inverse of the relative change in fluorescence.

2.2 Stereo reconstruction

The stereo reconstruction process requires that both cameras capture overlapping areas of the epicardium, hence their parallel alignment, shown in the schematic in

Figure 1. The stereo camera pair was jointly calibrated using images of a planar calibration checkerboard in a large variety of positions [6], of which samples are shown in Figure 2. We first resolve the intrinsic and extrinsic parameters of each camera, and then for the rotation and translation between the pair [5].

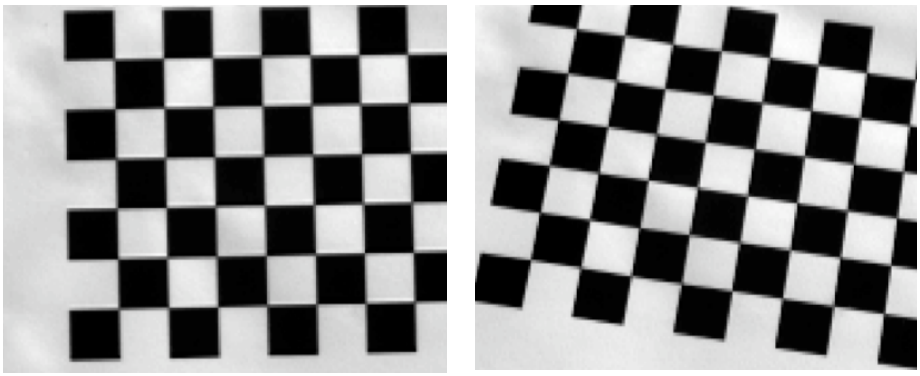

(a) (b)

Figure 2. Sample images of the calibration grid in approximately (a) fronto-parallel and (b) tilted and rotated views.

The camera calibration parameters were used to rectify all the stereo image pairs collected during fluorescence and normal imaging, so that point correspondences from matching image pairs could be found by searching along horizontal scan lines [4]. Normalized cross-correlation was used to compare the 11 x 11 patch centered at each pixel in the left rectified image, to candidate patches in the right rectified image, centered on the same horizontal scan line. For a pixel coordinate (x,y) in the left image, and stereo disparity estimate, d, the normalized correlation, ψ, can be calculated as:

$$\psi(x,y,d) = \frac{\sum_{i=-5}^{5}\sum_{j=-5}^{5}\left(I_{left}(x+i,y+j)\cdot I_{right}(x+i+d,y+j)\right)}{\sqrt{\left(\sum_{i=-5}^{5}\sum_{j=-5}^{5}I_{left}(x+i,y+j)\right)\cdot\left(\sum_{i=-5}^{5}\sum_{j=-5}^{5}I_{right}(x+i+d,y+j)\right)}} \qquad (\mathbf{1})$$

The validity of disparity estimates was then verified through the use of left-right consistency checking [8]. This process compares the disparities estimated when using the left image as the reference image during the correspondence search, against the corresponding disparities estimated when using the right image as the reference image. Under ideal circumstances, the estimated disparity values should vary by a sign change. However, half-occluded points that appear in one image of the stereo pair but not the other result in different disparity estimates depending on the reference image used. We identify image points as potentially half-occluded if the left-right consistency check produces disparity estimates for corresponding pixels that fall outside a tolerance of 2 to 3 pixels.

3 Results and Discussion

The optical imaging results shown below are taken from a single camera, although the corresponding results are available from the other camera in the stereo pair. We then present the results of the stereo reconstruction, and finally combine pseudo-colored fluorescence images with the 3D epicardium surface by texture mapping.

3.1 Optical Imaging

Illustrated in Figure 3 are AP waveforms for a 4s acquisition, shown after denoising with a soft-cubic filter (BV Analyzer, BrainVision Inc., Japan), beside a 2D projection of the activation pattern at one instance in time. The average duration of the action potential measured at 90% repolarization (APD90) is approximately 350ms, a reasonable value for healthy ventricular tissue paced at 1Hz. The depolarization front (in red) propagates from the bottom left of the heart toward the upper right side. The activation times can be represented by isochrones, lines connecting pixels of equal activation time. Figure 4 shows maps of pixel activation time from two different heart specimens paced with the stimulating electrode positioned inside the heart at the apex of the right ventricle.

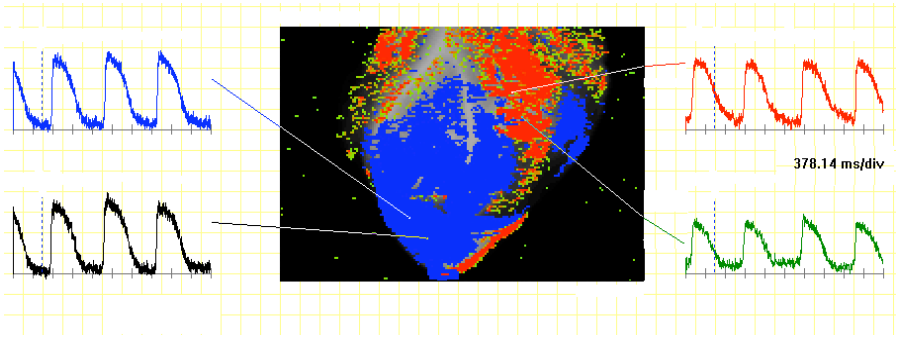

Figure 3. Action potential waveforms for four sample pixel locations of the epicardium. The red color overlay corresponds to the depolarized phase of the action potential, while the blue color corresponds to the repolarized phase.

3.2 Stereo Reconstruction

A stereo image pair under normal lighting conditions is shown in Figure 5(a) and (b). The target distances from the camera to the tissue fell in the range between 35 and 45cm, restricting the range of the disparity search to approximately 20 pixels. The disparity value that yielded the highest correlation value (which has a maximum of 1) in that range was chosen as the best disparity estimate. Disparity was used in turn to triangulate the 3D positions of each image point.

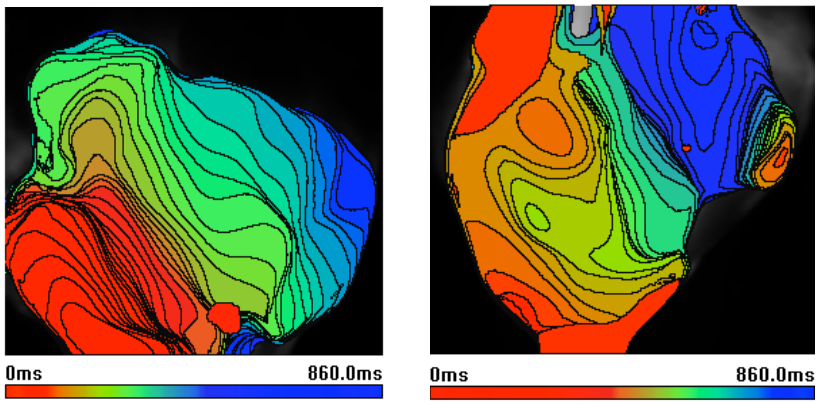

(a) (b)

Figure 4. Activation maps from two different hearts, isochrones 20ms apart.

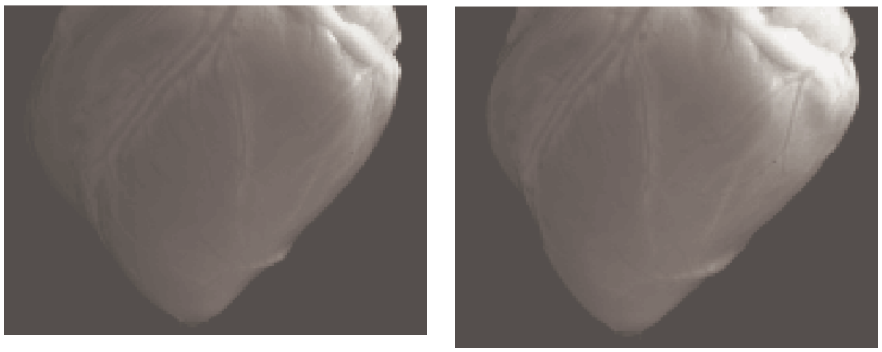

(a) (b)

Figure 5. Examples of the (a) left and (b) right stereo image pairs taken under normal lighting.

In order to verify the validity of point correspondence estimates, a grid pattern was projected onto the heart, as shown in Figure 6, producing a set of identifiable landmarks in the left and right images of the stereo pair. The pixels on the top left and bottom right points of each grid intersection point were marked for a set of 40 intersections in the left and right images of the gridded stereo pair. The manually selected disparity estimates were then compared against those of the fully automatic cross correlation-based technique applied to the non-gridded stereo pair shown in Figure 5. The resulting comparison yielded a mean difference of 1.62 pixels over the 40 test points, with a maximum difference of 3.48 pixels.

The range of camera to target distances used in our experiments lay between 38cm and 44cm, a single pixel of disparity produced differences in depth estimates between 1.62mm and 2.11mm, with decreasing accuracy as the distance from the camera increases. Manual correspondence marking in test images of the calibration grid was

also used to measure the accuracy of 3D distance measurement between points. Measurements of lengths along the planar grid's squares of up to 44mm near the center of the field of view in a roughly fronto-parallel orientation, were all within 0.5mm of the known grid dimensions.

The final disparity map obtained from the stereo pair of ungridded images under normal lighting conditions is shown in Figure 7(a). It is important to note that disparity values cannot be accurately estimated in non-overlapping image regions, such as those areas at the left and right borders of the heart. Furthermore, it is impossible to obtain valid disparity estimates in uniform image areas, such as the black background.

Areas of possible half-occlusion are detected by the left-right consistency check, and marked regions are overlaid upon the normally lit image in Figure 7(b). Notwithstanding the tendency of left-right consistency checking to produce a significant proportion of false-positives in natural images with primarily low-frequency characteristics [8], the left-right consistency check confirms the stereo system's limited accuracy in half-occluded areas that arise due to the curvature of the heart.

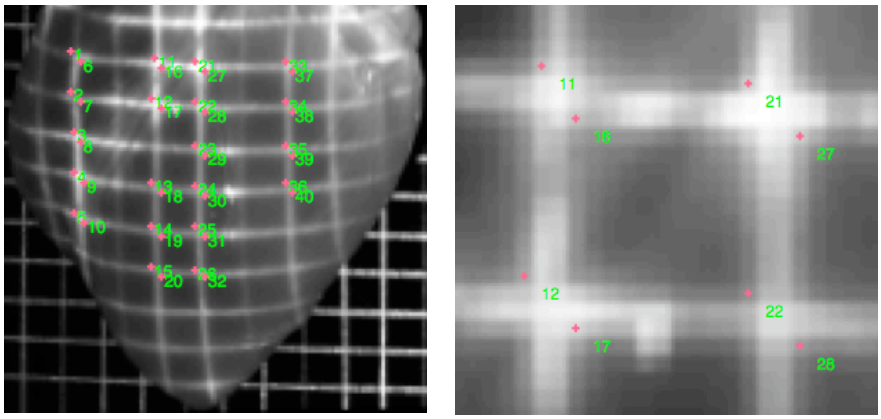

(a) (b)

Figure 6. (a) Full scale and (b) zoomed images of the heart with a grid projected onto it. Overlaid annotations illustrate the 40 manually marked image points used to assess the validity of the cross-correlation automatic point correspondence search.

Stereo reconstruction of the 3D surface using that image pair is shown in Figure 8(a) and (b), with plain shading to illustrate the surface shape, and texture mapped to show the surface under normal lighting conditions. Figure 8(c) and (d) show the reconstructed surface texture mapped with pseudo-colored activation maps. These activation maps shows how the activation spreads diagonally when paced from the apex of the RV, from lower left part of the hearts to the upper right section.

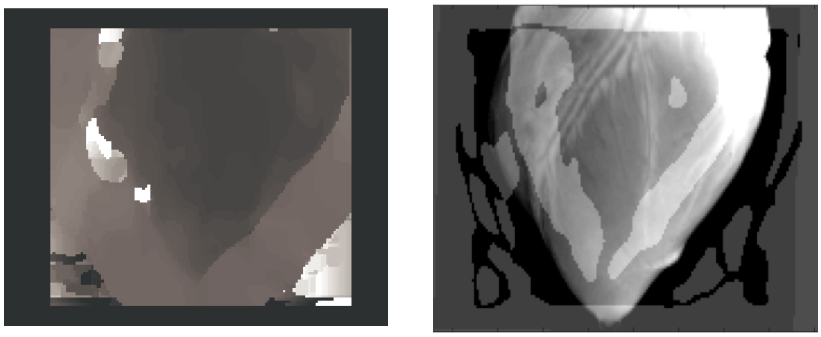

(a) (b)

Figure 7. (a) The disparity between corresponding points in the left and right images detected by the correspondence search is inversely proportional to the depth of each image point. (b) The left to right consistency check indicates which image regions provide accurate disparity estimates (shown at normal intensity) and which regions may not (shown at higher intensity), indicating that regions of high curvature may be poorly reconstructed.

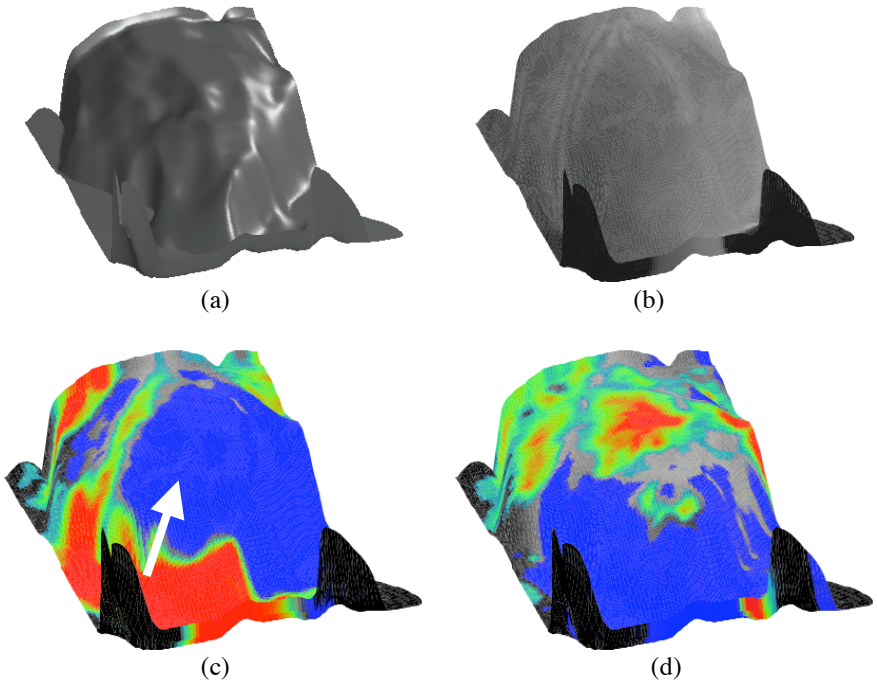

(a) (b)

(c) (d)

Figure 8. Renderings of the reconstructed 3D surface of the epicardium shown in Figure 5. In (a), the solid surface indicates the epicardial shape, while in (b) the surface is texture mapped with the intensities of a normally lit image. In (c) and (d) the propagation of AP is texture mapped onto the 3D surface for two instances in time. The white arrow in (c) indicates the direction of propagation.

4 Conclusion

In this work, we propose a stereo optical imaging configuration method to simultaneously recover the 3D epicardial geometry and estimate the electrical activation patterns derived from fluorescence images. Our results suggest that stereo reconstruction of the 3D epicardial surface is feasible for large hearts, comparable in size to human hearts, while avoiding the complex camera configuration required by existing work [3] for shape recovery. The technique enables the visualization and measurement of the AP propagation across the 3D geometry of the heart, providing a powerful tool for computer-aided diagnosis and for validating 3D simulations of cardiac electrical activity. Furthermore, this approach may provide more accurate measurements of electrophysiological parameters such as conduction velocity.

Future work will extend the optical imaging procedures to capture the entire epicardium by periodically rotating the heart by a small angle, then repeating reconstruction and fluorescence imaging. The stereo imaging procedure could be immediately improved by optimizing the distance between the stereo camera pair to reduce the area of half-occlusion, and by manufacturing the calibration grid with higher precision.

Acknowledgements

The authors would like to thank Dr. John Graham (Sunnybrook Health Sciences Centre, Toronto, Canada) for surgical preparation of the ex-vivo hearts, and Professor Jack Rogers (University of Alabama, Birmingham, USA) for valuable discussion regarding the optical imaging technique. This study was supported by funding from the Ontario Research and Development Challenge Fund, the Canadian Foundation for Innovation, and the Ontario Innovation Trust. Ms. Mihaela Pop is supported by a scholarship from the Heart and Stroke Foundation of Canada.

References

1. Efimov, I.R., Nikolski, V.P., Salama, G.: Optical imaging of the heart. Circulation Research 95(1) (2004).
2. Sung, D., Omens, J.H., McCulloch, A.D.: Model-based analysis of optically mapped epicardial activation patterns and conduction velocity. Annals of Biomedical Engineering 28(9) (2000).
3. Kay, M.W., Amison, P.M., Rogers, J.M.: Three-dimensional surface reconstruction and panoramic optical mapping of large hearts. IEEE Transactions on Biomedical Engineering 51(7) (2004).
4. Trucco, E., Verri, A.: Introductory Techniques for 3-D Computer Vision. Prentice-Hall (1998).
5. Bouget, J.Y.: Camera calibration toolbox for Matlab. http://www.vision.caltech.edu/bouguetj/calib_doc/index.html (2005).
6. Zhang, Z., A flexible new technique for camera calibration. IEEE Transactions on Pattern Analysis and Machine Intelligence 22(11) (2000).
7. Heikkila, J., Silven, O.: A four-step camera calibration procedure with implicit image correction. IEEE Conference on Computer Vision and Pattern Recognition (1997).
8. Egnal, G., Wildes, R.P: Detecting binocular half-occlusions: Empirical comparisons of five approaches. IEEE Transactions on Pattern Analysis and Machine Intelligence 24(8) (2002).